Maximum Radiated Emissions Evaluation for the Heatsink/IC Structure Using the Measured Near Electrical Field

Guangyao Shen, Sen Yang, Jingdong Sun, *Student Member, IEEE*, Shuai Xu, *Senior Member, IEEE*, David J. Pommerenke, *Fellow, IEEE*, and Victor V. Khilkevich, *Member, IEEE*

***Abstract*—Creating an equivalent field source is an efficient method for predicting radiated emissions from IC structures. In this paper, the maximum radiated emissions for a heat-sink/IC structure is predicted by creating an equivalent source from the measured electrical field (E-field) in the gap between the heatsink and IC. The E-field is detected by an E-field probe made of an open coaxial cable coated with absorbing material. A numerical model is built in the computer simulation technology microwave studio to obtain the maximum radiated field, where the measured E-field is used as a source to excite the heat-sink model. The evaluated maximum radiated field is in good agreement with the measured value; the error is within 7 dB up to 40 GHz for the source with phase, and 7 dB up to 10 GHz for the phaseless measurement.**

***Index Terms*—Equivalent principle, field transformation, maximized radiated field, probe calibration.**

I. Introduction

THE use of heat sinks is a common method to improve the heat dissipation of digital ICs. At the same time, heat-sinks are known to be electromagnetic interference (EMI) sources [1].

Many articles have been published that model the radiated emissions of heatsinks [1]–[6]. In [1] and [5], full-wave simulations were used to model the radiated emissions of a heatsink. In [6], the heatsink was modeled as a superposition of a patch antenna and a thick monopole. Then, the worst case maximum radiated field was obtained. The full-wave methods are generally highly accurate, but they require information about the source, which is usually not available. The worst-case estimations often are too pessimistic.

Another approach is to create an equivalent source using the Huygens principle and perform a near-field to far-field transformation [7]–[9]. Application of the Huygens principle implies measuring the tangential components of the EM field on a surface enclosing the source of EMI [10]. In [11], the near field was obtained on the surface completely enclosing the radiation structure. However in the case of the heatsink [see Fig. 1(a)], the measurement needs to be performed over both horizontal and vertical planes, which is difficult to accomplish.

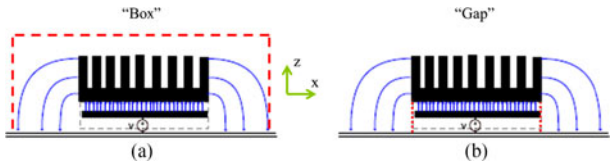

Fig. 1. Two methods to do field transformation.

In this paper, an alternative method of measuring only the vertical component of the electric field (E-field) in the gap between the heat sink and the ground plane [see Fig. 1(b)] is proposed, which greatly simplifies the measurement process by avoiding the need to change the probe orientation during scan and switching from the surface scan to the linear scan. The maximum radiated field is evaluated by the numerical model of the heatsink when it is driven by the measured electric near field source at the gap.

The proposed probe is essentially an asymmetrical dipole (or a monopole). Similar design was proposed before in [12]. The main contribution of the paper regarding the probe design is a use of absorber material to suppress the common-mode resonances. The proposed design allows us to build a relatively accurate broadband (up to 40 GHz) E-Field probe using thin semirigid cables (several mm outer diameter as opposed to 508 μm in [12]).

The structure of the article is the following. In Section II, the E-field probe structure and calibration method are given. In Section III, the electric near field measurement and transformation techniques are presented. The setup for the maximum far field measurement, and the validation of the predicted values, is introduced in Section IV. In Section V, the entire procedure is applied to a situation with active EMI sources (FPGA and clock IC).

II. E-Field Probe and Probe Calibration

A. E-Field Probe Structure

Probably the simplest way to detect electromagnetic fields is to use an open coaxial cable [12]. The cable essentially forms

Manuscript received October 27, 2016; revised February 13, 2017; accepted February 28, 2017. Date of publication April 6, 2017; date of current version May 25, 2017. This work was supported by the National Science Foundation under Grant IIP-1440110. *(Corresponding Author: Guangyao Shen.)*

G. Shen, S. Yang, J. Sun, D. J. Pommerenke, and V. V. Khilkevich are with the Department of Electrical Engineering, Electromagnetic Compatibility Laboratory, Missouri University of Science and Technology, Rolla, MO 65041 USA (e-mail: gs97b@mst.edu; sydgf@mst.edu; sunjing@mst.edu; david.hill@nist.gov; khilkevichv@mst.edu).

S. Xu is with the Huawei Technologies, Shenzhen 518129, China (e-mail: shuai.xu@huawei.com).

Color versions of one or more of the figures in this paper are available online at http://ieeexplore.ieee.org.

Digital Object Identifier 10.1109/TEMC.2017.2688325

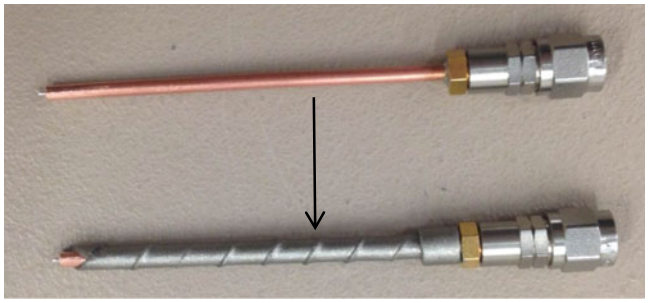

Fig. 2. E-field probe.

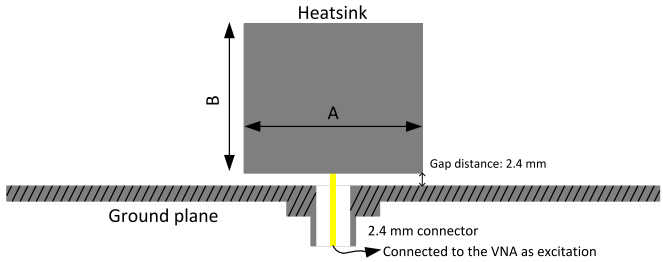

Fig. 3. Diagram of the setup at the excitation of the heatsink.

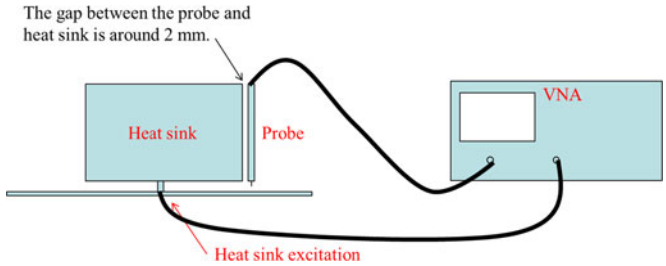

Fig. 4. Calibration setup.

a highly asymmetrical dipole antenna, with strong current on the outer surface of the cable shields. In antenna design, this current is usually suppressed by baluns or other similar devices [13]. Another way to eliminate this unwanted common mode current is to use a differential probe design [14]. Both methods are not very suitable for heat sink measurement. The balancing devices are difficult to build (especially the broadband ones), and the symmetrical differential E-field probes are not suitable to measure the vertical fields close to the metallic ground planes because of geometrical constrains. For example, if a probe similar to one described in [15] is used for the vertical-field measurements, its cables will have to run parallel to the PCB plane at a very close distance to it, where they would collide with the PCB components. Bending the cables might alleviate the problem somewhat, but the probe might lose symmetry.

Another popular approach to build the E-filed probes is the PCB design [16]. In this case the elements of a dipole are placed on the opposite sides of a 4-layer PCB. However in order to measure the vertical E-field component above a PCB of an electronic device the PCB of the probe needs to be placed parallel to the device PCB at a very close distance, which is again not possible because of the nearby components on the PCB.

Instead of complicated balancing techniques, the common mode current in the proposed design is suppressed by applying a flexible electromagnetic absorber (WX-A020) [17] to the coaxial cable, as illustrated in Fig. 2. The effect of the absorber on the common mode of the probe is discussed in the next section.

B. Probe Calibration

The probe is calibrated using a combination of measurement and simulation. For the calibration, a special structure was built containing a heat-sink driven by a coaxial cable (see Fig. 3).

Two heat sinks were used for the calibration (heat sink 1 with $A = 15$ mm, $B = 25$ mm; and heat sink 2 with $A = 27$ mm, $B = 25$ mm).

The probe tip height over the ground plane and the distance between the probe and the heatsink were kept the same during both the calibration and the DUT measurement (1 and 2 mm, respectively). Fig. 4 illustrates the process of the probe calibration.

Assuming the output voltage of the probe is proportional to the vertical component of the E-field in the gap between the heat sink and the ground plane, the probe factor can be defined as:

$$A = E_z^c / V_{\text{out}}. \tag{1}$$

The unknown E_z^c field at the gap across the position of the probe is obtained by the full-wave simulation of the heatsink (the model corresponds to Fig. 3). The probe load is nonreflective, which is ensured by the VNA calibration. Under this condition, the transmission coefficient from the heatsink port to the probe output can be written as:

$$S_{21}^c = \frac{V_{\text{out}}}{V_{\text{inc}}} \tag{2}$$

where V_{out} is the output voltage of the probe (which is equal to amplitude of the transmitted wave in the case of the nonreflective load) and V_{inc} is the incident voltage used in the full-wave simulation.

Therefore, the probe factor is calculated as:

$$A = E_z^c / (S_{21}^c V_{\text{inc}}). \tag{3}$$

The probe response S_{21}^c strongly depends on the resonances of the common mode current. An example of the responses for the probes with and without the absorbing material is shown in Fig. 5. As can be seen the response of the probe without the absorber contains multiple resonances, which makes the probe unusable, since the frequency and "amplitude" of the resonances strongly depend on the length and routing of the cable connecting the probe to the instrument. However, application of the absorber reduces the amplitude of the resonances, and hence, the probe factor uncertainty to proximately 3 dB, which is acceptable for many practical measurements.

The probe factor calculated according to (1) is in general dependent on the position of the probe along the side of the heat sink. To simplify data processing, an averaged probe factor was calculated by averaging A over many positions of the probe, and

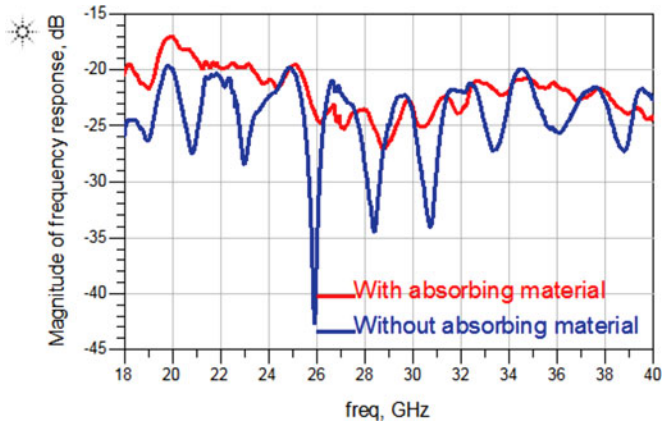

Fig. 5. Frequency response of the probe w/wo absorbing material.

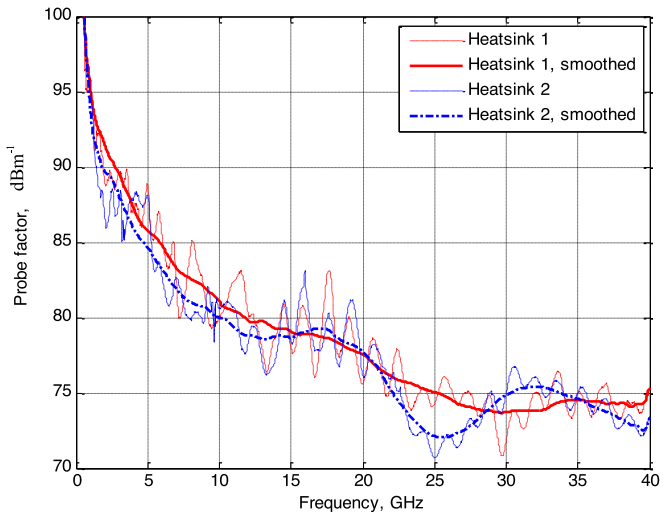

Fig. 6. Probe factors obtained on heat sinks 1 and 2.

smoothing the resulting curve to further suppress the effect of the residual common mode current, as shown in Fig. 6.

The difference between the averaged probe factors obtained using heat sinks 1 and 2 (see Fig. 4) is not more than 3 dB, which is accurate enough for many applications and thereby validates the proposed calibration procedure.

III. Near-Field to Far-Field Transformation

The electric near field generated by the heatsink was measured as shown in Fig. 7. The probe was mounted on a mechanical manipulator with three degrees of freedom. This allowed a fixed elevation to be maintained between the probe tip and the ground plane, while still allowing the probe to move parallel to the side of the heat sink.

The heat sink is excited by a VNA port, another port is used to detect the output signal of the probe. According to the definition of the probe factor above the E-Field between the heat sink and ground is calculated as

$$E_z = AV_{\text{out}}. \tag{4}$$

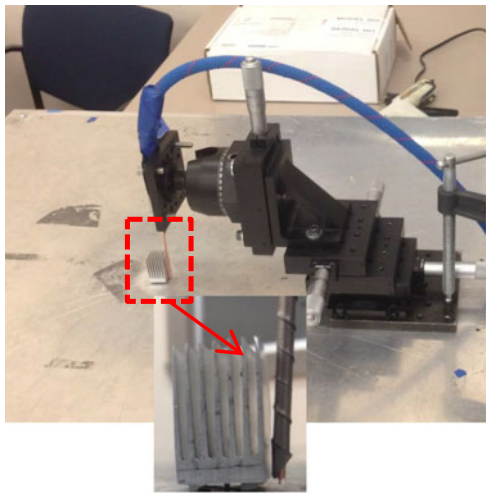

Fig. 7. Near field scanning setup.

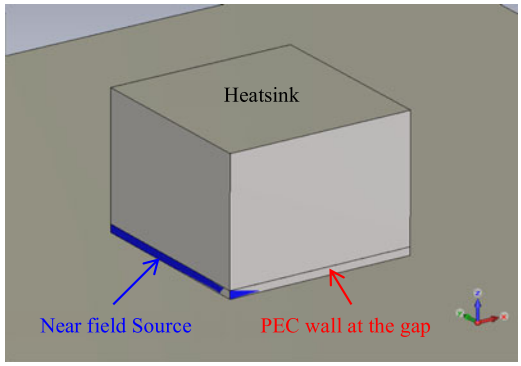

Fig. 8. Field transformation model in CST.

The output voltage of the probe is calculated as

$$V_{\text{out}} = S_{21}\, V_{\text{inc}} \tag{5}$$

where V_{inc} is assumed amplitude of the incident wave (set to the same value as excitation of the full-wave model), and S_{21} is the measured transmission coefficient.

The values of the E-Field measured at different locations are used to construct the near-field source in CST microwave studio. Since only the tangential E-Field components are measured, the inner volume of the source is filled with the PEC material to force the EM solver to calculate the missing tangential magnetic field components. The model in CST microwave studio is shown in Fig. 8. The maximum far-field was obtained using the CST time domain solver.

The phase of the E-Field at the gap between the heatsink and ground plane can be easily measured when the heat sink is driven by a VNA. However, if the measurement is performed using a spectrum analyzer, the phase is unavailable. To investigate the impact of phase on the accuracy, two versions of the near field sources were created – with and without the phase information.

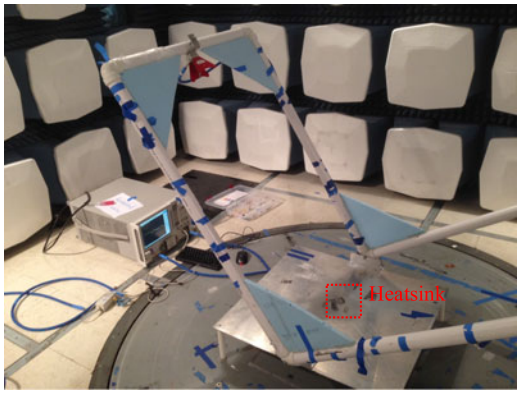

Fig. 9. Maximum far-field measurement setup.

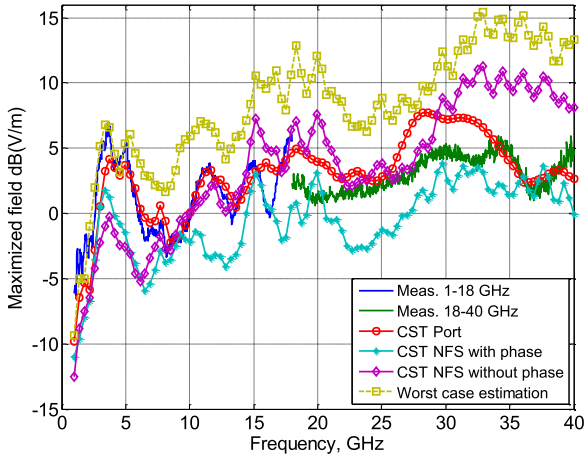

Fig. 10. Transformation results comparison.

IV. Maximum Far-Field Measurement Setup and Validation

The predicted EMI figure was validated against 1) the full-wave simulation model; 2) worst-case prediction according to [6], with conversion of the measured E-Field to the voltage between the heat sink and the ground plane; and 3) measurement.

To measure the maximum far-field, a special setup was built, as shown in Fig. 9. A horn antenna was placed 1.5 m away from the DUT and was attached to a plastic frame, allowing it to scan the DUT with respect to the polar angle. The azimuthal scan was performed by rotating the heatsink on its axis.

To cover the frequency range from 1 to 40 GHz, two broadband horn antennas were used: ETS Lindgren 3115 (1–18 GHz) and ETS Lindgren 3117 (18–40 GHz).

The azimuth angle was varied by a step of 10°. For each azimuth angle, a polar scan was performed by slowly (relative to sweep time of the instrument) moving the frame around its axis, so that the maximum field value was recorded. The final result was obtained by selecting the maximum values over all azimuthal positions.

The maximum electric far-field predicted by the near-field source method is compared in Fig. 10 to the measurement, the results of the three-dimensional (3-D) modeling ("CST port" curve), and the worst-case estimation according to [6].

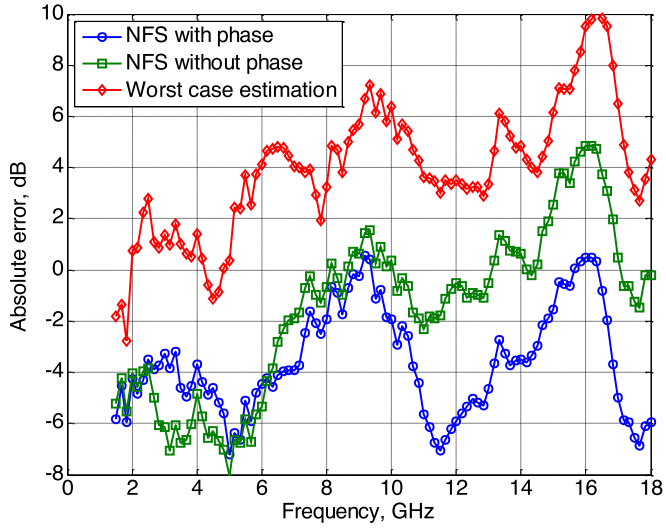

(a)

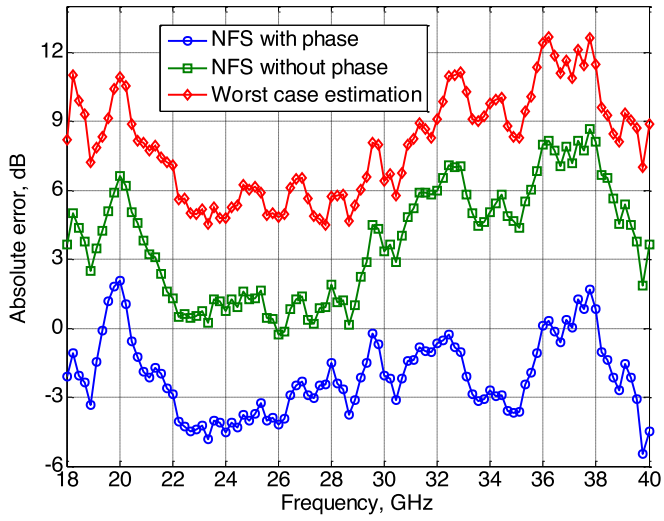

(b)

Fig. 11. Absolute error for 1–18 GHz (a) and 18–40 GHz (b).

For each of the predicted emission curves, the absolute error was calculated taking the measured data as a reference. It can be seen that the best accuracy is achieved if the phase is included into the equivalent source. In this case, the prediction accuracy is within 7 dB for the entire frequency range. If the phase is not used, the accuracy is within 7 dB up to 18 GHz and is within 9 dB from 18 to 40 GHz (see Fig. 11).

V. Active Hardware Validation

In order to validate the prediction methodology in the actual hardware case, the method was tested on two devices. The first test vehicle was a Cyclone III starter board (FPGA board). The FPGA ran a dummy code that implemented an array of adders. It was driven by its own internal PLL clock with a frequency of 467.857 MHz. To simulate the heat sink, an aluminum block was placed above the IC (see Fig. 12).

The near field at the gap was measured by the E_z probe and a spectrum analyzer (i.e., only the magnitude was measured),

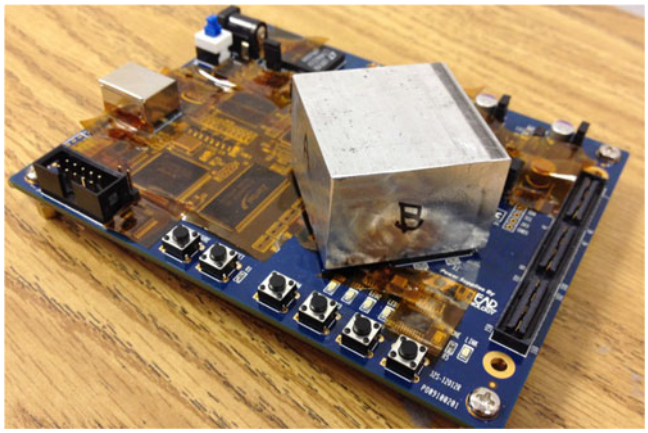

Fig. 12. Cyclone III starter board for validation from low frequency part.

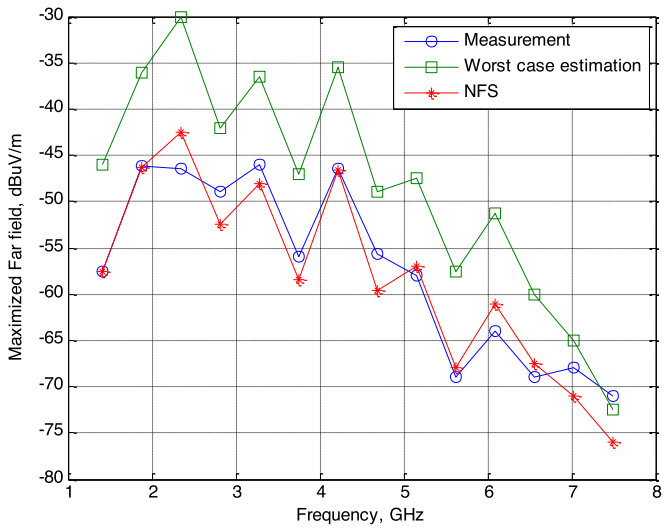

Fig. 13. Transformation result comparison for Cyclone III starter board.

and then, transformed to the far-field as described above. The far field for validation was measured in the setup shown in Fig. 9. The result of the transformation, along with the worst-case prediction, is shown in Fig. 13, where each marker represents a harmonic of the clock frequency. The transformation result has a good agreement with the measurement, as shown in Fig. 13. The error is within 5 dB for each harmonic. The frequency range (7.5 GHz) was limited by the sensitivity of the far-field measurement.

In order to test the method at higher frequencies, a 670 MHz clock IC (see Fig. 14) was also tested. This DUT allowed extending the frequency range up to 20 GHz.

The near field at the gap was measured with the electrical-field probe designed in Section I and a spectrum analyzer. The scanning results are illustrated by Fig. 15 (only two frequencies are shown), with blue dots representing the probing locations. The field between the measured points was obtained by interpolation.

The maximum far field was predicted by using the equivalent source created from the measured near field. The result is shown in Fig. 16.

Fig. 14. Clock buffer IC board for validation.

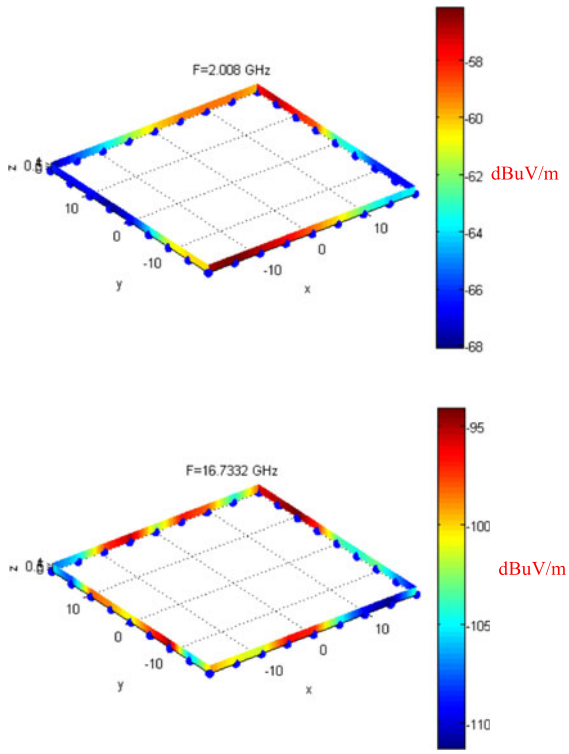

Fig. 15. Near-field 3-D visualizations for two frequencies.

The errors of the maximum field transformation for the heat sink/IC structure are within 7 dB up to 10 GHz. Above 10 GHz, the errors can reach 13 dB (see Fig. 17). The transformation accuracy for the active DUTs roughly agrees with the accuracy achieved in the passive case with no phase information (see Fig. 11). However, the errors are larger than expected at around 10.5 and 16.5 GHz. This effect can be explained by the following consideration. The increased errors correlate with the resonances of the heat-sink which is illustrated by the pink line in Fig. 17, representing the reflection coefficient of the heat sink measured during the probe calibration.

It could be that the probe is affected by the resonant structure nearby which adds uncertainty to the probe factor. Decisive identification of the accuracy limiting factors of the method requires additional investigation. However, as shown by results in

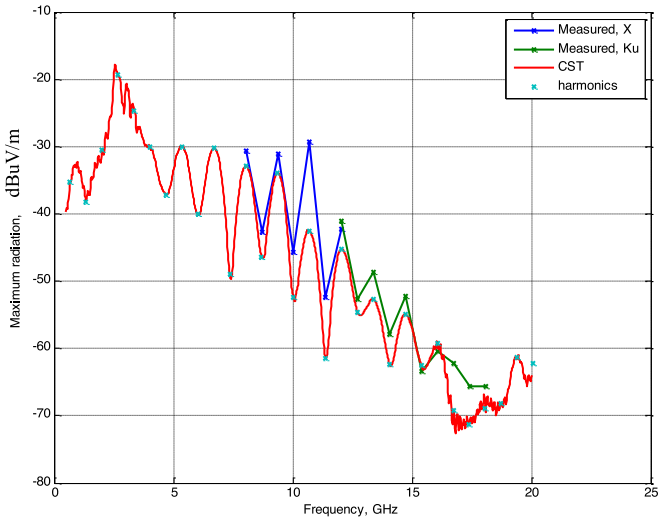

Fig. 16. Transformation result comparison for the clock signal board.

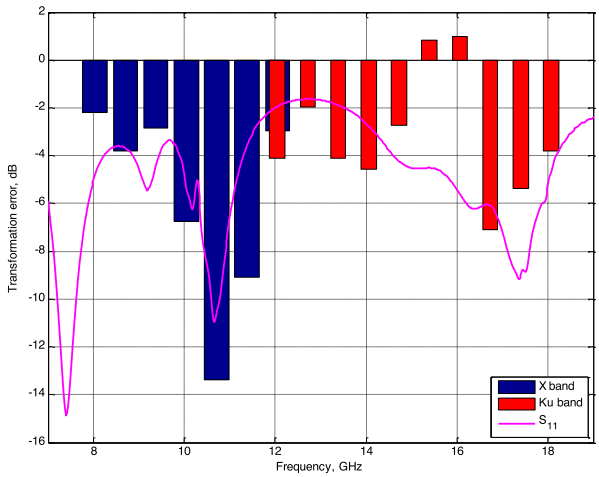

Fig. 17. Absolute error for the Clock buffer IC board.

Figs. 13 and 16, the method provides acceptable (7 dB) accuracy with the phaseless measurements using a spectrum analyzer up to 10 GHz.

VI. Conclusion

A design of a simple E-Field probe proposed. The probe can be used to measure the field in the gap between the heat sink and the PCB ground plane and predict the far-field radiation of the IC/heatsink. As shown by the measurements on the passive structures the proposed method can potentially provide 7 dB accuracy of the far-field prediction up to 40 GHz. The accuracy of the prediction on the active devices is lower, however no more than 7 dB error is achieved up to 10 GHz. The proposed measurement/transformation technique is relatively simple to use and can be used to avoid time-consuming far-field measurements in the anechoic chamber, as well as for the estimation of the far-field contributions of the individual ICs. Only one component of the E-Field is required for the field transformation and only a linear scan is needed to obtain the data.

References

[1] N. J. Ryan, D. A. Stone, and B. Chambers, "Application of the FD-TD method to modelling the electromagnetic radiation from heatsinks," in *Proc. 1997 10th Int. Conf. Electromagn. Compat.*, Sep. 1997, pp. 119–124.

[2] N. J. Ryan, D. A. Stone, and B. Chambers, "FDTD modeling of heatsinks for EMC," in *Proc. Int. Conf. Exhib. Electromagn. Compat.*, Jul. 1999, pp. 125–130.

[3] N. J. Ryan, B. Chambers, and D. A. Stone, "FDTD modeling of heatsink RF characteristics for EMC mitigation," *IEEE Trans. Electromagn. Compat.*, vol. 44, no. 3, pp. 458–465, Aug. 2002.

[4] S. K. Das and T. Roy, "An investigation of radiated emissions from heatsinks," in *Proc. 1998 Symp. IEEE Electromagn. Compat.*, 1998, vol. 2, pp. 784–789.

[5] K. Li, C. F. Lee, S. Y. Poh, R. T. Shin, and J. A. Kong, "Application of FDTD method to analysis of electromagnetic radiation from VLSI heatsink configurations," *IEEE Trans. Electromagn. Compat.*, vol. 35, no. 2, pp. 204–214, May 1993.

[6] X. He and T. H. Hubing, "A closed-form expression for estimating the maximum radiated emissions from a heatsink on a printed circuit board," *IEEE Trans. Electromagn. Compat.*, vol. 54, no. 1, pp. 205–211, Feb. 2012.

[7] H. Weng, D. G. Beetner, and R. E. DuBroff, "Prediction of radiated emissions using near-field measurements," *IEEE Trans. Electromagn. Compat.*, vol. 53, no. 4, pp. 891–899, Nov. 2011.

[8] G. F. Ricciardi and W. L. Stutzman, "A near-field to far-field transformation for spheroidal geometry utilizing an Eigen function expansion," *IEEE Trans. Antennas Propag.*, vol. 52, no. 12, pp. 3337–3349, Dec. 2004.

[9] L. W. Lai, J. Y. Liu, Y. Y. Wu, S. M. Wu, and M. C. Fu, "Near-field to far-field transformation with non-contacting near-field measurement by using Kirchhoff surface integral representation," in *Proc. 2015 Asia-Pacific Microwave Conf.*, Nanjing, China, 2015.

[10] A. Radchenko, J. Zhang, K. Kam, and D. Pommerenke, "Numerical evaluation of near-field to far-field transformation robustness for EMC," in *Proc. 2012 IEEE Int. Symp. Electromagn. Compat.*, Pittsburgh, PA, USA, 2012, pp. 605–611.

[11] F. D'Agostino, F. Ferrara, C. Gennarelli, R. Guerriero, and M. Migliozzi, "Probe compensated near-field to far-field transformation with helicoidal scanning for elongated antennas," in *Proc. 2007 19th Int. Conf. Appl. Electromagn. Commun.*, Sep. 2007.

[12] Y. J. Gao and I. Wolff, "A simple electric near field probe for microwave circuit diagnostics," in *Proc. 1996 IEEE MTT-S Int. Microwave Symp. Dig.*, Jun. 1996, vo1. 3, pp. 1537–1540, Paper TH3C- 4.

[13] W. L. Stutzman and G. A. Thiele, *Antenna Theory and Design*, 2nd ed. New York, NY, USA: Wiley, 1998.

[14] T. Koskinen, H. Rajagopalan, and Y. Rahmat-Samii, "Impedance measurements of various types of balanced antennas with the differential probe method," in *Proc. 2009 Int. Workshop IEEE Antenna Technol.*, Santa Monica, CA, USA, 2009.

[15] L. Bouchelouk, Z. Riah, D. Baudry, M. Kadi, A. Louis, and B. Mazari, "Characterization of electromagnetic fields close to microwave devices using electric dipole probes," *Int. J. RF Microw. Comput.-Aided Eng.*, vol. 18, pp. 146–156, 2008.

[16] G. Li, K. Itou, Y. Katou, N. Mukai, D. Pommerenke, and J. Fan, "A resonant E-field probe for RFI measurements," *IEEE Trans. Electromagn. Compat.*, vol. 56, no. 6, pp. 1719–1722, Dec. 2014

[17] "WX-A series datasheet," [Online]. Available: http://arc-tech.com

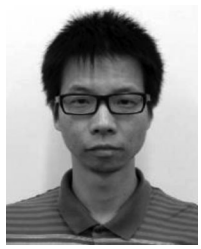

Guangyao Shen received the B.S. and M.S. degrees in electrical engineering from Huazhong University of Science and Technology, Wuhan, China, in 2008 and 2011, respectively. He is currently working toward the Ph.D. degree of electronic engineering in Missouri University of Science and Technology, Rolla, MO, USA.

He joined the Electromagnetic Compatibility Laboratory, Missouri University of Science and Technology, Rolla, in 2012. His research interests include IC immunity modeling, EMI prediction for Heatsinks, electric modules modeling for EMI and Immunity in auto vehicles, and three-dimensional Printing technology on the electromagnetic applications.

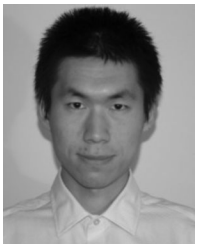

Sen Yang received the B.S. degree in electrical engineering from the University of Electronic Science and Technology of China, Chengdu, China, in 2012. He is currently working toward the M.S. degree in Electromagnetic Compatibility Laboratory, Missouri University of Science and Technology, Rolla, MO, USA.

In 2013, he joined Electromagnetic Compatibility Laboratory, Missouri University of Science and Technology, Rolla. His research interests include heatsink radiation prediction, IC ESD immunity modeling, and coupling path identification.

Jingdong Sun's, photograph and biography not available at the time of publication.

Shuai Xu (SM'16) received the M.S. degree in electrical engineering from Southeast University, Nanjing, China, in 2004.

He is currently a Principal Engineer at Huawei Technologies, Shenzhen, China. His primary research interests include passive intermodulation, radio frequency interference, electromagnetic compatibility modeling, meta-material based antenna design of next generation wireless communication, and high-frequency measurement techniques.

David J. Pommerenke (F'xx) received the Ph.D. degree from the Technical University Berlin, Berlin, Germany, in 1996.

After working at Hewlett Packard for five years, he joined the Electromagnetic Compatibility Laboratory, University of Missouri-Rolla, Rolla, MO, USA, in 2001, where he is currently a Professor. He has published more than 100 papers and is the holder of 11 patents. His research interests include EMC with emphasis on measurement and instrumentation, electronics, and immunity of electronic circuits, for example, electrostatic discharge.

Victor V. Khilkevich (M'08) received the Ph.D. degree in electrical engineering from Moscow Power Engineering Institute (Technical University), Moscow, Russia, in 2001. He is currently an Assistant Professor at the Missouri University of Science and Technology, Rolla, MO, USA. His primary research interests include microwave imaging, automotive electromagnetic compatibility modeling, and high frequency measurement techniques.